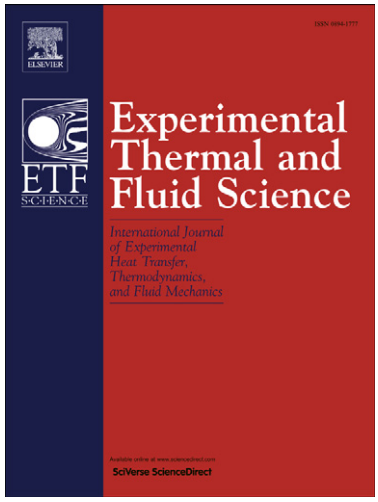

Experimental study of soot particle fouling on ribbed plates. Applicability of the critical local wall shear stress criterion

Concepción Paz, Eduardo Suárez, Miguel Concheiro, Jacobo Porteiro

PII: S0894-1777(12)00192-6
DOI: http://dx.doi.org/10.1016/j.expthermflusci.2012.07.008
Reference: ETF 7777

To appear in: *Experimental Thermal and Fluid Science*

Received Date: 23 February 2012
Revised Date: 5 July 2012
Accepted Date: 6 July 2012

Please cite this article as: C. Paz, E. Suárez, M. Concheiro, J. Porteiro, Experimental study of soot particle fouling on ribbed plates. Applicability of the critical local wall shear stress criterion, *Experimental Thermal and Fluid Science* (2012), doi: http://dx.doi.org/10.1016/j.expthermflusci.2012.07.008

Experimental study of soot particle fouling on ribbed plates. Applicability of the critical local wall shear stress criterion

Concepción Paz[a]*, Eduardo Suárez[a], Miguel Concheiro[a], Jacobo Porteiro[a]

[a] Escuela de Ingeniería Industrial, University of Vigo, Lagoas Marcosende 9 CP- 36310 Vigo, Spain

*Corresponding author: C. Paz, E-mail:cpaz@uvigo.es, Tel.: +34 986 813 754, Fax: +34 986 812 201

E-mail addresses: suarez@uvigo.es (E. Suárez), mconcheiro@uvigo.es (M. Concheiro), porteiro@uvigo.es (J. Porteiro)

Abstract

This article examines the notion of critical wall shear stress as the key control parameter of the local fouling removal process. In this study, an experimental setup was developed for measuring fouling on enhanced surfaces. Specifically, the experimental configuration consists of a forced convection plate heat exchanger containing a one-pass rectangular channel with two ribbed plates arranged in a symmetrically staggered manner. The exhaust gases flow by the rib-roughened sides of the plates, and the flat sides can be cooled with water from the independent external coolant circuit.

As a result of soot particle deposition from exhaust gases, a layer of fouling is deposited over the ribs. After asymptotic conditions were reached during the tests, detailed fouling thickness measurements were conducted. The dimensionless particle relaxation time during these tests was determined to be in the range of 0.3-10. The measurements were then complemented with a numerical analysis. In particular, the local wall shear stress was calculated using a commercial computational fluid dynamics (CFD) software package.

The fouling thickness profiles deposited over the ribs and the local critical shear stress values were compared and discussed for two different geometries. The results obtained clearly support the idea that critical wall shear stress is an appropriate criterion for facilitating the understanding of the local behaviour of fouling deposits.

Keywords: fouling thickness; rib; particle deposition; critical shear stress; soot

1. Introduction

The Euro policies are the European automotive antipollution standards. In recent years, more stringent requirements associated with exhaust gas emissions have led to the development of a series of devices designed to reduce emissions. These devices must function under extreme conditions and therefore require a high degree of engineering to successfully address aspects such as material selection, thermal and mechanical stress, pressure pulses, and heat transfer. One of the biggest challenges that must be overcome when designing such devices is that of the damage caused by fouling [1].

The fouling in exhaust gas systems is usually associated with particle deposition. There is general agreement regarding the main consequences of fouling, namely, a reduction in thermal transmission [2] and an increase in pressure losses [3].

Moreover, increasing the compactness of equipment is always a goal in the automotive industry. It has been well established that the performance of heat exchangers can be substantially improved by augmentative techniques that reduce the exchanger size and increase the exchanger power capacity. In particular, Manglik and Bergles [4] identified 13 such techniques that can be divided into the two main categories of active techniques, which require an external power supply, and passive techniques, which do not. Passive heat transfer enhancement technologies have been extensively studied in the past [5-7] as well as in recent years [8, 9]. The first practical enhancements of heat transfer were developed over 50 years ago [10]. Examples of enhanced surfaces can be found within compact heat exchangers, nuclear reactors, solar air heater ducts, chemical processing plants, and electronic devices.

The utilisation of obstacles is a common way of achieving intensification of the heat exchanger. Different types of obstacles have been developed, including dimples, pin-fins, perforated baffles, winglet vortex generators, and surface ribs [11]. The placement of repeated ribs periodically spaced along the flow direction of channel surfaces is one of the most commonly utilised techniques for obstacle-based heat exchanger intensification [9]. The periodic penetration of the ribs causes the separation and reattachment of the boundary layer, which promotes turbulent heat transfer and generates large-scale secondary flows. Moreover, the upstream rib wake region creates the effect known as shading. The wake formation and the separation point of a heat exchanger are influenced by its Reynolds number and rib shape.

The study of ribbed surfaces is not a new subject. The first studies involving two opposite ribbed walls were focused on the reattaching effect and the optimisation of all of the geometrical parameters involved

in surface design [6, 12, 13]. Most of these published papers were experimental studies aimed at determining the best Nusselt number correlation fit.

Geometric parameters, such as the pitch-to-height ratio (p/e), the rib-height-to-plate-spacing ratio (e/H), and the shape of the rib, play an important role in the system behaviour [6, 9, 12]. If the ribs reach a considerable height relative to the channel dimensions, the effect of the blockage ratio can also be important.

Fouling was not usually considered in these studies. In this study, an experimental layout was designed to measure the thickness of the fouling layer on enhanced surfaces that is produced by exhaust gas systems under operating conditions. Previous data from the literature [14, 15] and our own analysis [16] suggest that particle deposition is the primary mechanism controlling the fouling process. In fouling dominated by particles, several researchers, such as Messerer et al. [17] and Grillot and Icart [14], demonstrated the asymptotic evolution of deposits.

The growth of the deposited matter is controlled by the equilibrium between deposition and removal. Deposition mechanisms, such as sedimentation, diffusion, interception, electrostatic attraction, inertial impaction, gravitational settling, and thermophoresis, strongly depend on the size of the particles. In diesel exhaust gases, soot particles typically range in size from 10^{-8} to 10^{-5} m [15].

The particle deposition velocity is usually divided into three regimes, depending on the particle relaxation time t_p^+. If $t_p^+ < 0.1$, the deposition is considered to be controlled by diffusion (and thermophoresis if there are temperature gradients), whereas the deposition is considered to be governed by inertia if $0.1 < t_p^+ < 10$, with significant potential effects from turbophoresis and lift, and the deposition velocity falls into the impact regime if $10 < t_p^+$, [18].

After being deposited onto walls, particles can be removed and detached, sometimes returning to the main flow. This erosion process, described by Epstein [19], has not received adequate attention. Removal processes include mechanisms such as turbulent bursts, impacts, rolling, and scrubbing actions and have been proposed to be strongly linked to velocity [20].

The importance of wall shear stress as a removal parameter has been clear since the initial analysis by Kern and Seaton [21] and was later confirmed by Freeman [22]. The notion of critical wall shear stress was introduced in the filtration literature [23] but is not commonly used in this context.

The critical wall shear stress was proposed as a more local removal control parameter than the critical velocity by Paz et al. [16]. The critical wall shear stress was evaluated and compared with the fouling

thickness observed on cylindrical probes. In this case, values of dimensionless relaxation time varying from 0.1 to 1. The probes were well suited for identifying the thermophoretic effect.

In the present paper, the experimental layout conditions led to Re number ranged from 3 x 10^4 to 4 x 10^4, and the dimensionless particle relaxation time t_p^+ ranged from 0.3 to 10, therefore, thermophoretic effects should be smaller [18]. These ranges were chosen to extend previously obtained results [16]. In addition, the new test equipment introduces several dynamical features of the flow, thereby creating an environment more similar to that found in real heat exchangers.

Within the proposed experimental layout, different ribbed plates were fouled under the actual working conditions of a diesel exhaust device. The local depths of the obtained fouling layers were measured and were related to the critical wall shear stress concept. The results obtained extend the value of the removal criteria in the particle deposition field.

2. Experimental set-up

The main components of the bench test device were specifically designed to study the fouling deposition process on exhaust gas recirculation (EGR) systems. The new layout was integrated into the facility that was developed in the study discussing the fouling of cylindrical probes [16]. The exhaust gas lines and measurement section of this layout are shown in Fig. 1.

The gases used in this study were produced with a CGM10DW generator set composed of a Lombardini LDW 702 and a single pole alternator. In this system, gases were exhausted from a two-cylinder engine of 686cc working at 3000 rpm loaded with an adjustable resistive load which in this test varied near 6 kVA. The engine supplied a constant mass flow of roughly 60 kg/h with a temperature at the entrance of the experimental setup of 650 K that could be controlled through the resistive load.

All of the details regarding the control system, measurement devices, and working conditions can be found in the study by Paz et al. [16]. The design of the experimental device was based on a one-pass rectangular channel with two ribbed plates placed in a symmetrically staggered arrangement through which the exhaust gases flow. The resulting configuration yielded a plate heat exchanger with forced convection. A schematic of the assembly is shown in Fig. 2.

The main components of this heat exchanger were the two aluminium ribbed plates. The coolant housing was formed by a one-piece aluminium box. The rest of the components were commercial gaskets, screws, and thread. The connections with the exhaust lines were composed of stainless steel AISI 316L and

connected the probe to cylindrical shells with an inner diameter of 53 mm. The connections allowed the assembly to be placed at any angle transverse to the flow direction, thereby enabling the evaluation of the effects of gravity on fouling.

The exhaust gases flow over the rib-roughened plate sides, and the flat plate sides can be cooled with water from the coolant circuit. Fig. 2 shows the fouling on the probe in detail.

With the goal of evaluating the value of the critical wall shear stress, two different periodically ribbed plates were designed. These plates were arranged in a symmetrically staggered manner, as shown in Fig. 3. The two designed ribbed plates had the same total length (L) of 200 mm, width (W) of 50 mm, and number of ribs (N) of 11. The material for both was aluminium, which was processed by standard milling machinery using a standard commercial surface finish (IT8), with a conductivity λ of 210 W/mK.

The geometrical characteristics of each ribbed plate are shown in Fig. 3 and Table 1. The only difference between the plates was the rib severity, as the ratio of rib-height-to-plate-spacing was increased by 62.5% from the lower to the higher rib. These two plates were denoted as plate A and plate B, respectively.

Two different rib severities were used to obtain a better analysis of the results. For a more detailed study regarding the effects of geometrical rib parameters on the fouling deposited, a wider range of rib parameters would be necessary.

The layout design was chosen for several reasons. First, the ribbed plates can be mounted with an easily interchangeable system, thereby allowing the utilisation of any rib geometry with the same conditions. In addition, each fouled plate can be readily extracted for weighing and measurement. The chosen working conditions generated the desired range of Reynolds numbers and t_p^+ values and reproduced the typical conditions of the enhanced surfaces that are actually used in heat exchangers. The chose of aluminium was with the idea of increasing the thermal gradient during the cooled experiments in order to improve the possibilities of thermophoretic deposition to contribute to the overall fouling rate, therefore the differences between the cooled and the uncooled tests, if existent, should be more clear. Furthermore, the recent tendency towards more compact and efficient heat exchangers is leading some applications towards the use of aluminium in EGR heat exchangers.

Using the 95% confidence level method recommended by Moffat [24], the overall experimental uncertainty was calculated as follows:

fluid temperatures, ±0.35 ºC to 100 ºC and ±0.95 ºC to 400 ºC [25]

air flow rate, 0.5 ±1 % of the measured values

water flow rate, ±1.5 % of the measured values

fouling thickness, ±2.5 μm

fouling mass, ±0.001 g, accuracy balanced

2.1 Experimental procedures

All tests started with a warm-up period, which continued until the engine temperature and rpm were stabilised. The exhaust gas flows through a bypass circuit in this step. Once uniformity in working conditions was obtained, the measurement main gas line was opened, and the testing time was properly began.

Asymptotic evolution was assumed, as is typical in studies of fouling by particle deposition [14, 19, 26-28]. Under this assumption, each test was conducted until all experimental parameters reached a steady level to ensure stabilised conditions. Thus, the end of each test was determined by the effectiveness loss of the heat exchanger probe in the system. To ensure that the final conditions were achieved, a minimum of 100 hours for each test was established.

The process of dismantling was accomplished through the removal of two screws from two threaded holes on both ends of each plate. This process was performed somewhat delicately, as it was a difficult operation due to the low consistency of the residue and its tendency to crumble. This observation is consistent with the hypothesis that fouling is controlled by soot particle deposition.

The procedure followed in each test is listed below:

Before starting the test, clean conditions were ensured, and each plate of the heat exchanger to be probed was weighed.

The engine was started and ran until the entire system was warm.

The exhaust gas started to flow through the measurement section.

During the test, the temperature, pressure drop and thermal efficiency were monitored.

Once all of the control parameters reached a stable steady state, the test was completed.

The fouled plates of the heat exchanger were then carefully removed and weighed.

The thickness of the residue deposited on the tested plates was measured using an image scanner system with a resolution of 9800dpi, which is equal to a pixel size of approximately 2.5 μm. The measurement operation was repeated twice over the two ribbed sides of each plate to minimise

the error of the measurement process. Later, all points were numerically smoothed to obtain an average profile.

At the end of each test, all of the components were cleaned in an ultrasound cleaning bath.

The exhaust gas composition, and general engine behaviour was controlled during the test period with periodical particles and gas emission control. The measured values during the tests averaged 12.4 %CO_2, 168.7 ppmCO, 11.2 ppm THC, 319.6ppm NOx, and a particle concentration of 47.1 mg/m^3N which was derived from an average opacity measurement of 2.0 FSN and calculated through a model proposed by Magin et al [29].

As mentioned above, the parameter used to determine the end of each experiment was the thermal efficiency of the probes. In all cases, the efficiency followed the same pattern, and the conventional definition of efficiency [30], Eq.(1), was used:

$$\varepsilon = \frac{T_{g_{in}} - T_{g_{out}}}{T_{g_{in}} - T_{c_{out}}} \quad \textbf{(1)}$$

The experimental protocol was designed to analyse and compare the fouling on ribbed plates. All of the probed plates were characterised by a gas mass flow rate of 60 kg/h, a coolant temperature of 90 ºC (or uncooled), and an exhaust gas temperature at the entrance of the test section of approximately 650K.

3. Results

A total of 10 plate tests were performed. No significant differences between the upper and lower plates were observed. Moreover, a test in which the plates were rotated 90 degrees was conducted without notable changes. Therefore, the effects of gravity on plate results appear to be negligible. This result is in agreement with previously published fouling studies with small particles (r_p<5 μm) [31].

The results obtained for the fouling mass deposited during the experiments are summarised in Table 2.

The typical fouled rib appearance is shown in Fig. 4. In this image, three different areas are clearly distinguishable. These areas are identified as I, II, and III, in the sense of flow. The profile of fouling layers over the full length of each plate was measured. To clearly analyse these results, the fouling depth on each rib was compared. The resultant deposition on each rib, numbered by flow direction, is summarised in Fig. 5. As shown, the region prior to the rib (Area I) shows a small fouling in its beginning which gets thicker towards the end of the region. Probably this is due to the creation of a recirculation

flow that reduces the shear stress and allows the arrival of particles (by any of the mechanisms described earlier) with a low removal counterpart. Area II corresponds to the least fouled zone, which is attributable to the dominant erosion on the exposed to the flow side of the rib. Also the boundary layer thickness of this area is reduced and therefore the region is more affected by bulk properties. This effect joined to the geometry produce an increase of particle impacts by inertia which competes with a strong removal force Thus in this region, the appearance of the fouling matter was somewhat different. The area III is associated to stronger turbulent effects which correspond to the rib wake area. Due to the separation of the main flow, this region is characterized by the arrival of smaller particles mainly due to diffusion and thermophoresis while the arrival due to inertia should be minimal and the low erosion leads to a higher overall fouling. Due to the aforementioned differences in the flow between Area I and Area III the appearance of the residue was smoother in area I and rougher in area III.

The evolution of each fouled rib profile with length was measured, and no notable differences were found. To reduce the uncertainty of the experiments, the thickness of the fouling layer on each rib was averaged. The mean value or an equivalent profile of the fouling layer on each probe was then analysed. The fouling layer thickness measurements for plate A are shown in Fig. 6, and Fig. 7 depicts these measurements for the more severe ribbed plate B. As shown in these figures, several common features were observed in all cases. The profiles of the fouling layers appear to follow a similar pattern. When the profiles are oriented so that the gas flow is from left to right, the region less affected by fouling is clearly identifiable on the left incident side of the rib. In each case, the back side showed the greatest thickness.

4. Numerical simulation

To evaluate the local critical wall shear stress concept, it was necessary to calculate the wall shear stress on the two ribbed plates tested.

Many experimental studies of ribbed studies have been performed that focused on obtaining correlations [9, 12]. These results were obtained through general analyses of mean flow parameters. However, to our knowledge, there is no detailed experimental measurement or correlation that accurately provides the flow shear stress on ribbed surfaces, likely because the cost of an experimental apparatus to measure local wall shear stress data was unacceptably high. These types of results are typically obtained with the support of computational fluid dynamics (CFD) tools.

4.1 Mesh generation

The simulations were performed with the software Fluent 13.0 (ANSYS, Inc.). The geometry and the mesh of the tested geometries were generated using GambitTM and TGrid, which are the pre-processing modules of the Fluent code.

To solve the near-wall viscous region with precision, a 25-cell prismatic boundary layer was created. The size was adjusted to attain a y^+ value on the adjacent wall cell of approximately 1, and a linear growth model was used to achieve a smoother transition to bulk cells.

The solution obtained was analysed for different mesh resolutions to ensure grid independence in accordance with the CFD Best Practice Guidelines [32]. The transverse, longitudinal, and boundary layer mesh size parameters were studied separately. The transverse convergence was reached with a cell size rate ($L/\Delta x$) on the order of 10^2, corresponding with a cell size of 2 mm, so it was not restrictive. The stability of longitudinal size results was obtained with a cell size rate on the order of 10^3 (cell size 0.2 mm), as observed in Fig. 8a. For the boundary layer, dimensionless wall distances lower than 2 appear to be sufficiently accurate, as observed in Fig. 8b. As a result, the final 3D cell number used was approximately 5 x 10^6 cells.

4.2 Numerical model

Once the resulting mesh model passed all quality checks, the mesh was exported to Fluent, where the boundary conditions and physical properties were determined and calibrated.

Both anterior and posterior to the real domain, adiabatic virtual ducts were added to obtain a developed inlet profile and prevent reverse flow, respectively. The experimental exhaust gas mass flow of 60 kg/h was imposed as a mass flow inlet condition and a pressure outlet on the exit section. All of the external walls were supposed to be adiabatic, corresponding to the isolated configuration employed in the test. The coolant flow was substituted by an equivalent heat transfer coefficient at the bulk temperature. This assumption is common in detailed heat exchanger one-sided simulations [33].

Turbulent heat transfer was modelled using the Reynolds analogy to turbulent momentum transfer. Due to the simple geometry and flow of the turbulent RANS-based modelling approach, the standard k-ε model was used. The viscosity-affected near-wall region was resolved by enhanced near-wall treatment using the standard k- ε two-layer model of Wolfshtein incorporated into the Fluent code [34].

Because of the low Mach numbers associated with the working conditions of typical exhaust gas devices, the incompressible-ideal-gas law option was used to model density variations with temperature. The viscosity was computed following the Sutherland formulation, and a segregated solver was adopted.

The software employed allows the utilisation of four different interpolation schemes. After convergence, first-order upwind schemes were achieved, and the second-order scheme QUICK was then used for all equations. The results obtained are shown in Fig. 8b, in which the rates with final mean wall shear stress are compared between both numerical schemes. In addition, all computations were performed in double precision.

The convergence was judged by monitoring the scaled residuals, following the Fluent recommendation of maintaining at least 10^{-3} for all variables. Moreover, several key parameters were monitored, such as the outlet pressure, temperature, and mean and maximum wall shear stresses. The computation was stopped after all of these criteria were achieved and the second-order flow solution converged. This modelling strategy has been utilised in previously published studies [35]. An Intel ® Xeon ® Quad-Core E5530 2.4-GHz cluster with 96 GB of RAM was used for the computation. The average time per simulated case was approximately 20 h.

5. Discussion

5.1 Mean values

In the tested case of engine exhaust gas passing through heat exchangers, increases in the mean velocity of the gas resulted in decreases in the amount of fouling deposition. The majority of the removal mechanisms, such as the impact of particles, turbulent bursts, round stress, and scrubbing action, are related to the fluid velocity. This relationship was experimentally demonstrated in previously published studies [36, 37].

The amount of residue deposited on B-type plates was approximately 30% lower than that on A-type plates. This effect is clearly detectable in Table 2 and is also reflected in the fouling thickness, as shown in Figs. 6 and 7.

This result is consistent with the conventional concept of critical velocity due to the reduction of the gas-free section. As a consequence, the mean particle velocity increases from the A- to the B-type plates. The different shapes of the ribs make difficult to quantify this increase. Using the hydraulic diameter based on the rib peaks distance, the increase in mean particle velocity could be calculated to be approximately

15%. As mentioned, a more realistic reduction in the mean particle velocity from B- to A-type plates, based on the real gas volume in each case, is approximately 8%.

The increase in the ratio of rib height to plate spacing of 62.5% from the lower to the higher ribbed plates results in a 30% reduction in deposition. Thus, although the influence of the velocity on the resultant deposited fouling is clear, the quantification of this effect is complex. The concept of local critical wall shear stress instead of critical velocity as a parameter for the control of the fouling removal process simplifies the comparative analysis, and provides the important local concept.

An analysis of previous research regarding fouling in engine exhaust systems highlights the importance of the effects of the temperature gradient on the overall fouling layer. The importance of thermophoresis has been exhaustively studied, particularly with soot particles [17, 38], and this phenomenon has been shown to be most relevant for small particles [39]. The thermophoretic effect was result in a mean mass increase of approximately 50% under the conditions used for our previous experiments [16].

Based on the results obtained in this study, the effect associated with temperature was almost imperceptible. The average fouling mass in cooled and uncooled plates is primarily constant. The thickness, shape, and extent of fouling remained practically unchanged in the presence of the thermal gradient.

The equivalence of results with and without temperature gradients is consistent with our initial expectations. The particle deposition regime for this experiment is a key aspect of the explanation for this lack of a thermophoretic effect. The designed layout and the chosen working conditions placed the range of the dimensionless particle relaxation time t_p^+ between 0.3 and 10 for the typical exhaust particle size.

In contrast to our previous study [16], in this experiment, the work area in the typical v-shaped deposition velocity described by Guha et al. [18] was translated. Thus, the mechanism controlling deposition was translated to a more inertially dominant regime in which thermophoresis is a minor or even negligible factor.

5.2 Critical wall shear stress

It has been proposed that rolling is the major removal mechanisms and some good results have been obtained based in this assumption [40]. As particles are far from spherical, this rolling mechanisms cannot be considered as a perfectly physical description of the process taking place, however it seem to accurately describe the main forces involved in the process. Under this assumption, the critical flow

condition was defined as the mean flow velocity at which the rolling moment (*RM*) is equal to unity. The *RM* compares the hydrodynamic rolling moment with the adhesion resting moment [41].

Based on this concept, the critical shear stress τ_w^* was proposed as a removal parameter by Paz et al. [16]. This study attempted to establish a local explanation for the fouling profiles of the probes in relation to the shear stress patterns.

The critical shear stress was defined as the shear stress at which the rolling moment is equal to unity. Therefore, shear stress values higher than the critical value result in the rolling of deposited particles and their consequent movement along the wall. Given the initial assumption above, the more particle deposition predominates as the primary fouling process, the more representative critical shear stress will be as a removal parameter.

The critical wall shear stress was calculated for the entire range of particle diameters. For a given particle diameter, the critical wall shear stress τ_w^*, can be obtained. This evaluation was accomplished using the process previously detailed by Paz et al. [16].

The critical wall shear stress corresponding to the working particle diameter range was calculated, and these values were compared with the mean wall shear stress. The resulting ratios τ_w/τ_w^* are depicted in Fig. 9a.

In this figure, nearly half of the ratios exceeded 100 %, indicating that the particles of the corresponding diameters had a wall shear stress higher than the critical value; thus, rolling action was present, and the removal rate was high. The rate was similar for A- and B-type ribbed plates, although the experimental results clearly show greater removal, or lower deposition, for the A-type ribbed plates.

Using the detailed results obtained by simulations, the critical wall shear values were compared with the wall shear stress throughout the full ribbed plate surfaces. These results (Fig. 9b), which demonstrate a greater difference between the two differently ribbed surfaces, agree with experimental values.

The removal rate observed in this study is clearly higher than that observed in previous studies of cylindrical probe fouling [16], in accordance with the predicted extension of flow regime working conditions. The removal rates derived from the simulation were of the same magnitude as the mean observed rates, which reinforces the reliability of the simulation results.

Figs. 10 a and 10 b present detailed diagrams of the wall shear stress rates throughout the two studied ribbed plates, A and B, respectively, which are again oriented with the gas flow from left to right. In the same manner as was noted for the mean analysis, ratios larger than 100% for a given particle diameter

result in the prevention of deposition through the rolling mechanism. This removal action most likely affects particles of other sizes by directly impacting them; thus, areas with high shear stress rates tended to have smaller fouling thicknesses. This result agrees with the measurements shown in Figs. 6 and 7.

The deposition thickness on the incident side of the rough rib plate should be zero given the rate values for the working conditions; however, these rates alone cannot completely explain the residue thickness, as was mentioned above.

A visual comparison of the rates shown in Figs. 10 a and 10 b makes it clear that greater rates are seen in the latter because of the greater rib severity present in that case. The profile shapes of the shear stress rates suggest differences in the deposition tendencies of particles of different sizes, an observation that is consistent with the visual fouling distinctions depicted in Fig. 4.

The wall shear stress values and the results for average fouling thicknesses from both analysed plates are superimposed in Figs. 11 and 12.

The wall shear profile shows a clear maximum on the left (incidence) rib side and much lower values on the right (back) rib side. The shear stress values behaved similarly in both cases, thus the critical values too. The minimum fouling thicknesses were found approximately where the maximum shear stress was observed, at which point the critical shear stress was exceeded for the larger particles. The thickness peaks coincided with the rib shadow zone, where the minimum shear stress was observed.

Further analysis of the residue thickness profiles revealed that there was a peak near the -4-mm-length area in all cases. These peaks appear in the last flat area just before the start of the incident rib side. This area coincides with low values of wall shear stress, although it lies just before the area associated with the maximum wall shear stress values. One potential explanation for why this depth is higher than expected is that in this area, there was an increase in the particles available to be attached due to their proximity to a high-erosion region. The particles shed from the area of greatest wall shear stress (on the incident rib side) would be reincorporated into the flow but would not have enough energy to reach the mainstream flow. These particles trapped in the boundary layer with low shear stress will therefore be deposited near the -4-mm previously deposited fouling layer.

Other removal mechanisms, such as water condensation, chemical reactions, and deposition of hydrocarbons, are known sources of inaccuracies in this study. In addition, calculations of the actual shear stress on the ribbed surface should take into consideration the changes in surface geometry caused by the fouling thickness. Nevertheless, these rates show the important role of a local parameter in at least

partially explaining the final fouled layer profile. Thickness measurements and visual inspection confirmed the pattern of behaviour that was detailed above.

6. Conclusions

A plate heat exchanger was built and coupled successfully to a system capable of providing engine exhaust gas flow. This system allowed the measurement of exhaust gas fouling behaviour on enhanced surfaces.

The designed layout allowed the measurement of deposited layer thickness, weight, shape, and distribution on ribbed plates of different severities. The experimental procedure guaranteed that all of the measurements were collected under asymptotic conditions.

Due to the versatility of the setup, different angular positions of the assembly and coolant configurations were tested. The effects of gravity on the deposited layers were found to be negligible.

Little influence of thermophoresis was found under the specific conditions tested, as particle deposition appeared to be largely governed by inertial mechanisms. The contrast observed between this result and the importance of thermophoresis found in the previous study highlights the sensitivity of fouling mechanisms to changes in the working conditions. Increasing the severity of the ribbed surface led to a reduction in fouling deposition under the same gas and particle flow conditions.

A more detailed analysis of the numerical results contributed to the understanding of the experimental fouling results.

The range of work by the erosion criteria was defined, has been extended successfully. In particular, the detailed profiles, peaks and valleys of the measured fouling were discussed, evaluated and compared with critical wall shear stress values. These results were analysed from both global and local perspectives, and they illustrate the importance of local effects on the deposition of particles.

In all cases, the minimum deposition depth occurred on the incident side of the rib, coinciding with the maximum wall shear stress and therefore the greatest removal rate. The shape of the fouling profiles across the ribbed plates was explained based on the effect of the local critical wall shear stress on removal rates.

The results and analyses conducted in this study pave the way for studies of various aspects of fouling, including rib severity, rib arrangement, temperature gradients, differences in operating conditions,

instantaneous measurements, and numerical modelling of fouling. These experiments would clarify several of the uncertainties identified in this study.

The depth of the fouling layer deposited on ribbed plate surfaces exposed to diesel exhaust gases showed a clear correlation with local shear stress profiles. The critical wall shear stress was therefore shown to be a very powerful criterion for the quantification of local erosion.

Nomenclature

e	rib height (m)
H	plate spacing (m)
L	total length (m)
N	rib number, dimensionless
p	pitch (m)
r_p	particle radius (m)
Re	Reynolds number, $\mathrm{Re} = \frac{\rho u D_h}{\mu}$, dimensionless
T	temperature, (K)
t	plate thickness (m)
t_p^+	particle relaxation time, $t_p^+ = \frac{2\rho_p r_p^2 \rho_g u_\tau^2}{9\mu}$, dimensionless
W	width (m)
y^+	wall distance, dimensionless

Greek symbols

	thermal conductivity (W/mK)
Δx	cell size (m)
ε	thermal efficiency, dimensionless
τ_w	wall shear stress (Pa)

Subscripts and superscripts

c	coolant
g	gas

in	inlet
out	outlet
A	plate type A
B	plate type B
∞	free-stream (far away from the walls)
$*$	critical

References

[1] H. Teng, G. Regner, Characteristics of Soot Deposits in EGR Coolers, Society of Automotive Engineering, 01-2671 (2009).
[2] T.R. Bott, L.F. Melo, Fouling of heat exchangers, Experimental Thermal and Fluid Science, 14 (1997) 315-315.
[3] J.E. Hesselgreaves, The efect of system parameters on the fouling performance of heat exchangers, Proceedings of the 3rd UK National Conferenceon Heat Transfer and1st European Conference on Thermal Sciences, Institute of Chemical Engineering, (1992).
[4] R. Manglik, A. Bergles, Enhanced Heat and MassTransfer in the New Millenium: a review of the 2001 literature, Enhanced Heat Transfer, 11 (2004) 87-118.
[5] R. Webb, Performance evaluation criteria for use of enhanced heat transfer surfaces in heat exchanger design, International Journal of Heat and Mass Transfer, 24 (1981) 715-726.
[6] J.C. Han, Heat Transfer and Friction in Channels With Two Opposite Rib-Roughened Walls, Journal of Heat Transfer, 106 (1984) 774-781.
[7] B.H. Chang, A.F. Mills, Turbulent flow in a channel with transverse rib heat transfer augmentation, International Journal of Heat and Mass Transfer, 36 (1993) 1459-1469.
[8] Y. Xing, S. Spring, B. Weigand, Experimental and numerical investigation of impingement heat transfer on a flat and micro-rib roughened plate with different crossflow schemes, International Journal of Thermal Sciences, 50 (2011) 1293-1307.
[9] T. Giovanni, Effect of rib spacing on heat transfer and friction in a rectangular channel with 45° angled rib turbulators on one/two walls, International Journal of Heat and Mass Transfer, 54 (2011) 1081-1090.
[10] A.E. Bergles, Enhanced Heat Transfer: Endless Frontier, or Mature and Routine?, 6 (1999) 79-88.
[11] R.L. Webb, N.H. Kim, Principles of Enhanced Heat Transfer, Taylor and Francis, 2004.
[12] J.C. Han, L.R. Glicksman, W.M. Rohsenow, An investigation of heat transfer and friction for rib-roughened surfaces, International Journal of Heat and Mass Transfer, 21 (1978) 1143-1156.
[13] F. Burggraf, Experimental heat transfer and pressure drop with two-dimensional turbulence promoter applied to two opposite walls of a square tube, in: A. Bergles, R. Webb (Eds.) Augmentation of Convective Heat and Mass Transfer, ASME, New York, 1970, pp. 70-79.
[14] J.M. Grillot, G. Icart, Fouling of a cylindrical probe and a finned tube bundle in a diesel exhaust environment, Experimental Thermal and Fluid Science, 14 (1997) 442-454.
[15] D.B. Kittelson, Engines and nanoparticles: a review, Journal of Aerosol Science, 29 (1998) 575-588.
[16] C. Paz, E. Suárez, A. Eirís, J. Porteiro, Experimental evaluation of the critical local wall shear stress around cylindrical probes fouled by diesel exhaust gases, Experimental Thermal and Fluid Science, 38 (2012) 85-93.
[17] A. Messerer, R. Niessner, U.Poschl, Thermophoretic deposition of soot aerosol particles under experimental conditions relevant for modern diesel engine exhaust gas systems, Journal of Aerosol Science, 34 (2003) 1009-1021.
[18] A. Guha, Transport and Deposition of Particles in Turbulent and Laminar Flow, Annual Review of Fluid Mechanics, 40 (2008) 311-341.
[19] N. Epstein, Fouling: Technical aspects, Fouling of heat transfer equipment, (1981) 31-53.
[20] G. Lepperhoff, M. Houben, Mechanisms of deposit formation in IC engines and heat exchangers, Society of Automotive Engineering, 931032 (1993).
[21] D.Q. Kern, R.E. Seaton, A theoretical analysis of thermal surface fouling, British Chemical Engineering, 4 (1959) 258-262.
[22] W.B. Freeman, J. Middis, H.M. Müller-Steinhagen, Influence of augmented surfaces and of surface finish on particulate fouling in double pipe heat exchangers, Chemical Engineering and Processing: Process Intensification, 27 (1990) 1-11.
[23] M.C. Aubert, M.P. Elluard, H. Barnier, Shear stress induced erosion of filtration cake studied by a flat rotating disk method. Determination of the critical shear stress of erosion, Journal of Membrane Science, 84 (1993) 229-240.
[24] R.J. Moffat, Describing the uncertainties in experimental results, Experimental Thermal and Fluid Science, 1 (1988) 3-17.
[25] DIN/IEC 751 Reference platinum precision resistance thermometers, in, International Electrotechnical Commission, 1983.

[26] H.M. Müller-Steinhagen, J. Middis, Particle Fouling in Plate Heat Exchanger, Heat Transfer Engineering, 10 nº4 (1989) 30-36.
[27] B. Thonon, S. Grandgeorg, C. Jallut, Effect of Geometry and Flow Conditions on Particulate Fouling in Plate Heat Exchangers, Heat Transfer Engineering, 20, N 3 (1999).
[28] T.R. Bott, C.R. Bemrose, Fouling on the gas-side of finned tube heat-exchangers, Journal of Heat Transfer, (1983) 178-183.
[29] M. Lapuerta, F.J. Martos, M.D: Cárdenas, Determination of light extintion efficiency of diesel soot from smoke opacity measurements, Measurement Science and Technology 16 (2005) 2048-2055.
[30] F.P. Incropera, D.P. Dewit, Fundamentals of heat and mass transfer, Wiley, 1996.
[31] M.M. Sharma, H. Chamoun, D.S.H.S.R. Sarma, R.S. Schechter, Factors controlling the hydrodynamic detachment of particles from surfaces, Journal of Colloid and Interface Science, 149 (1992) 121-134.
[32] European Research Community on Flow Turbulence and Combustion. E.R.C.O.F.T.A.C. Best Practice Guidelines, in, 2000.
[33] M.C. Paz, A. Eirís, E. Suárez, C. Castaño, Heat transfer Enhancement in EGR coolers with internal corrugated tubes, in, 2007.
[34] ANSYS, Fluent user guide, ANSYS Inc., Lebanon, NH, in, 2008.
[35] F. Baetke, H. Werner, H. Wengle, Numerical simulation of turbulent flow over surface-mounted obstacles with sharp edges and corners, Journal of Wind Engineering and Industrial Aerodynamics, 35 (1990) 129-147.
[36] M.S. Abd-Elhady, S. Abd-Elhady, C.C.M. Rindt, A.A.v. Steenhoven, Removal of gas-side particulate fouling layers by foreign particles as a function of flow direction, Applied Thermal Engineering, 29 (2009) 2335-2343.
[37] M.S. Abd-Elhady, T. Zornek, M.R. Malayeri, S. Balestrino, P.G. Szymkowicz, H. Müller-Steinhagen, Influence of gas velocity on particulate fouling of exhaust gas recirculation coolers, International Journal of Heat and Mass Transfer, 54 (2011) 838-846.
[38] A.D. Eisner, D.E. Rosner, Experimental studies of soot particle thermophoresis in nonisothermal combustion gases using thermocouple response techniques, Combustion and Flame, 61 (1985) 153-166.
[39] M. Abarham, J. Hoard, D. Assanis, D. Styles, E. Curtis, N. Ramesh, Review of soot deposition and removal mechanisms in EGR coolers, Society of Automotive Engineers, 2010-01-1211 (2010).
[40] M.S Abd-Elhady, M.R. Malayeri, H. Müller-Steinhagen, Fouling Problems in Exhaust Gas Recirculation Coolers in the Automotive Industry Heat Transfer Engineering, 32 (2011) 248 - 257.
[41]F. Zhang, A. Busnaina, M. Fury, S.-Q. Wang, The removal of deformed submicron particles from silicon wafers by spin rinse and megasonics, Journal of Electronic Materials, 29 (2000) 199-204.

List of figures

List of tables

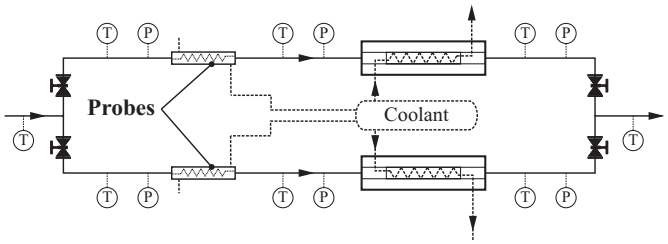

Fig. 1: Schematic of the measurement section.

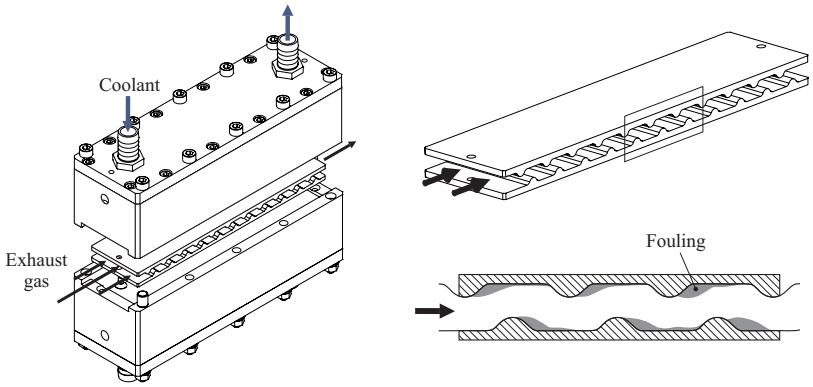

Fig. 2: Schematic of the assembly of the fouled plates.

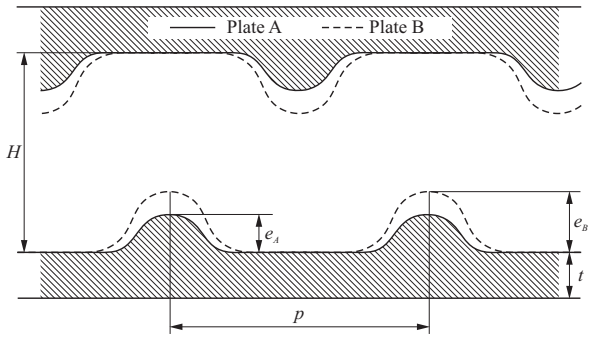

Fig. 3: Schematic of the designed ribbed plates.

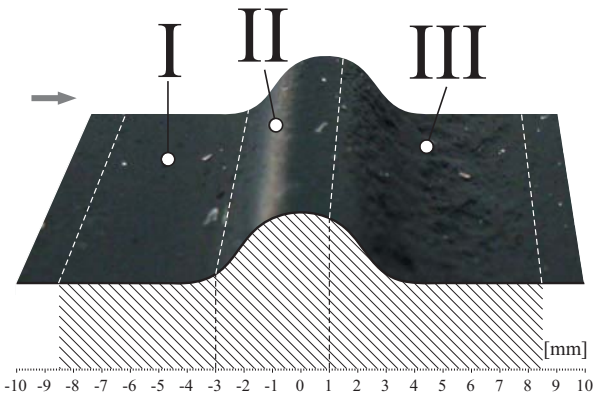

Fig. 4: Appearance of fouling deposited on a rib.

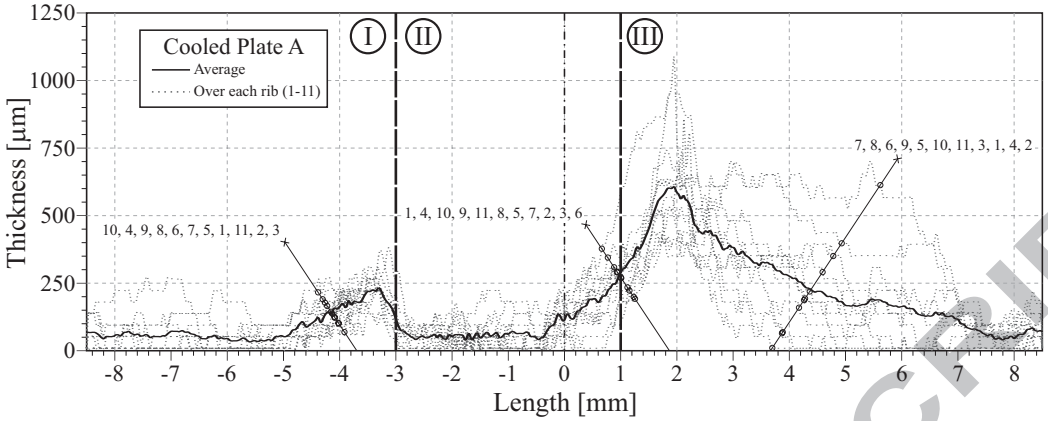

Fig. 5: Fouling thickness and average depth for each rib.

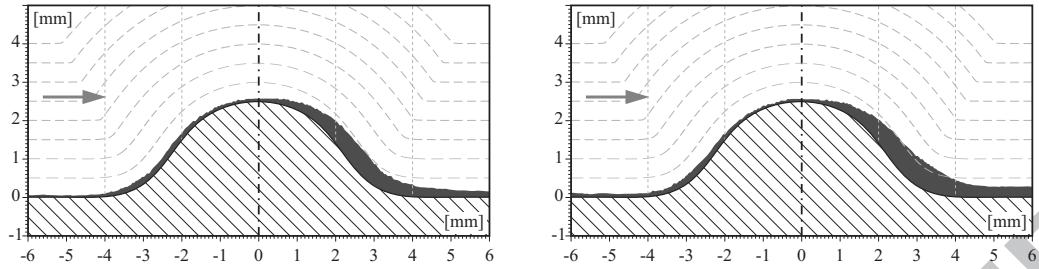

(a) Cooled plate (b) Uncooled plate

Fig. 6: Fouling thickness of the A-type plates.

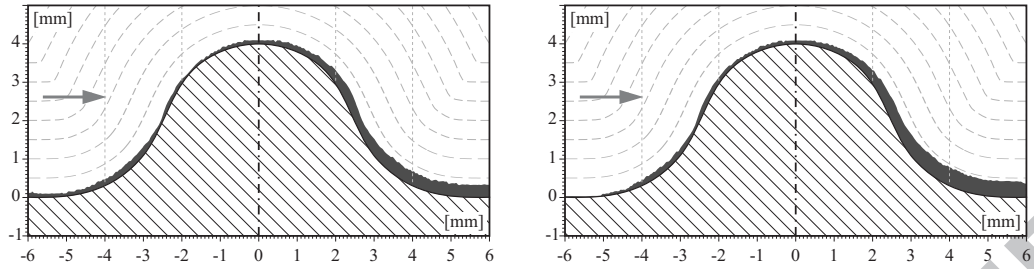

(a) Cooled plate

(b) Uncooled plate

Fig. 7: Fouling thickness of the B-type plates.

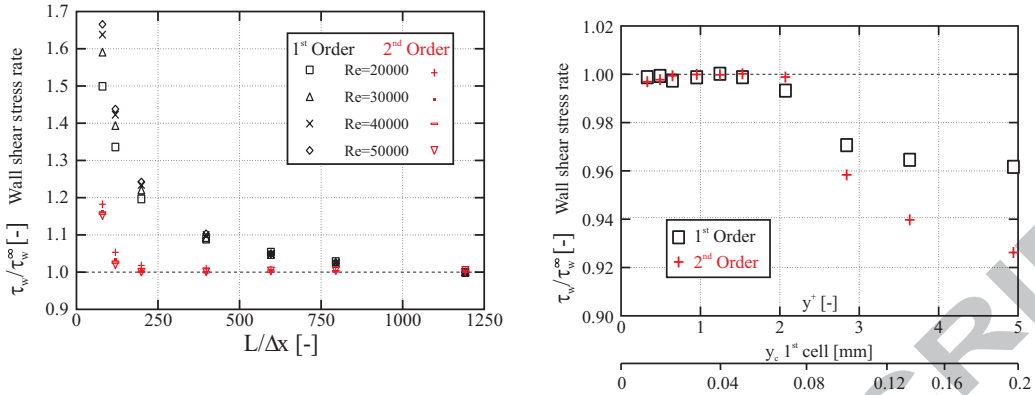

(a) Longitudinal cell size convergence

(b) Boundary layer convergence

Fig. 8: Grid convergence study results.

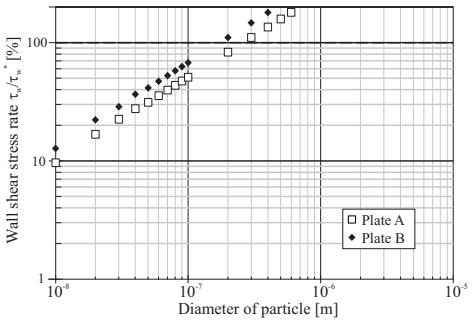

(a) Mean wall shear stress rate

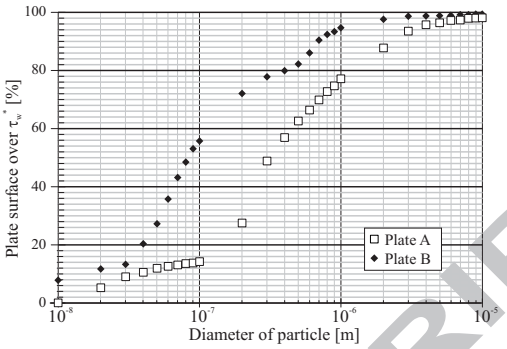

(b) Plate surface over τ_w^*

Fig. 9: Mean versus local measurements of critical parameters.

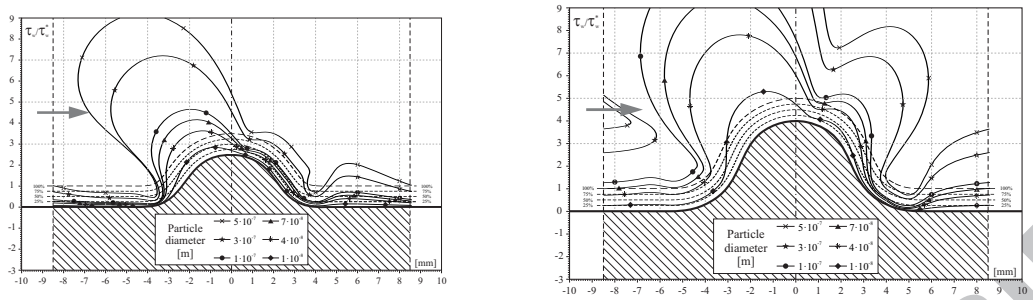

(a) Plate A

(b) Plate B

Fig. 10: Critical wall shear stress rates.

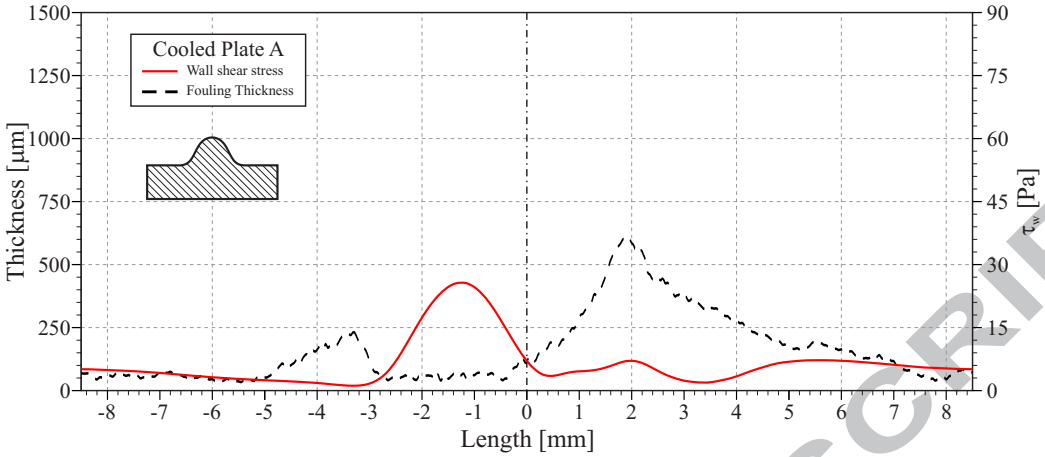

Fig. 11: Fouling thickness results superimposed on the wall shear stress values of cooled Plate A.

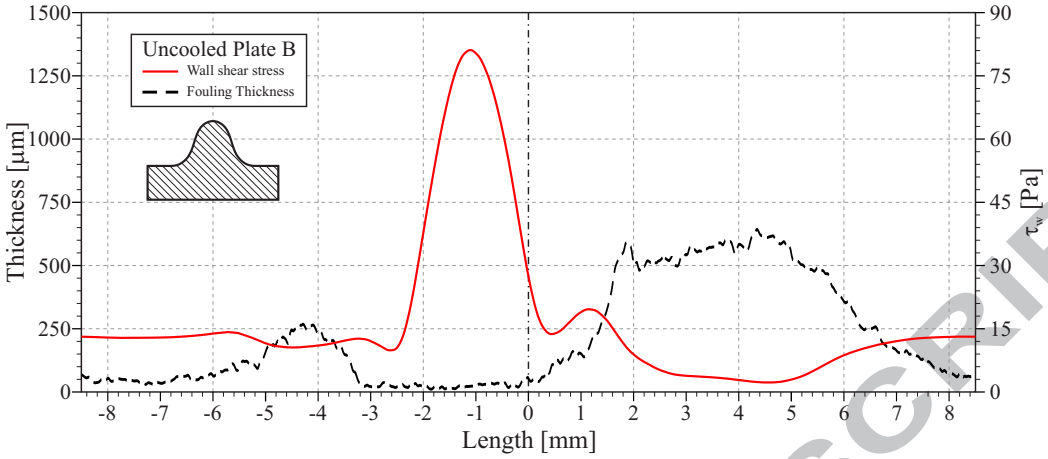

Fig. 12: Fouling thickness results superimposed on the wall shear stress values of uncooled Plate B.

Table 1: Measurements of ribbed plates (mm).

	Pitch, p	Rib height, e	Plate thickness, t	Plate spacing, H
Plate A rib	17	2.5	3	14
Plate B rib	17	4	3	14

Table 2: Mass deposited on the plates.

	Plate A			Plate B	
	Experimental mass (mg)			Experimental mass (mg)	
Cooled	140	340	210	140	120
Uncooled	120	340	190	190	160

Experimental layout developed to investigate fouling deposited on ribbed surfaces

Fouling thickness measurements were done after asymptotic conditions reached

The measurements were complemented with a CFD analysis

Critical wall shear stress aids to understand the local behaviour of the soot layer